

**PAPER • OPEN ACCESS** 

# Multi-device analysis of energy loss duration and pellet penetration with implications for shattered pellet injection in ITER

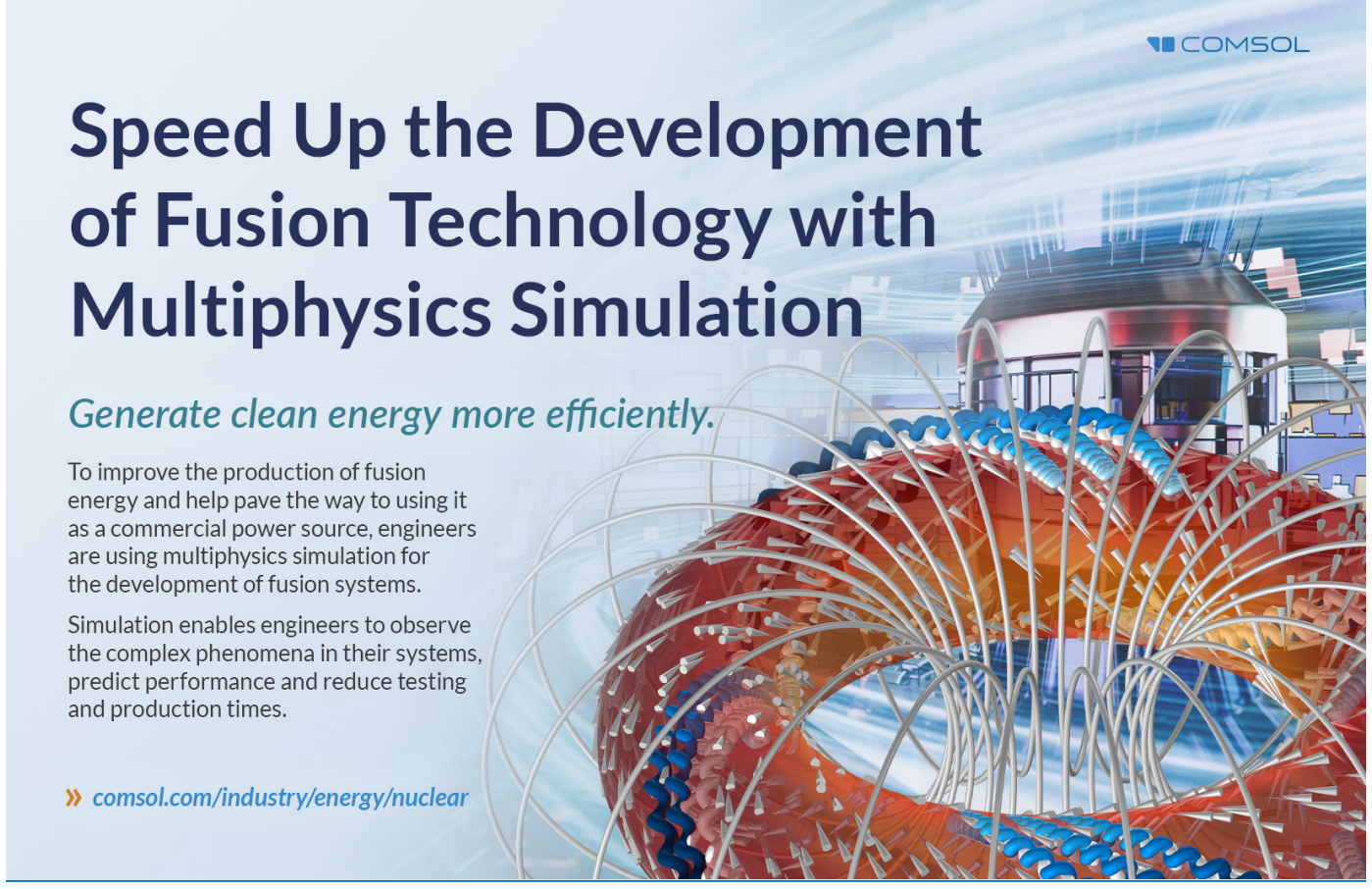
To cite this article: G. Bodner et al 2025 Nucl. Fusion 65 066010

View the article online for updates and enhancements.

# You may also like

- Axial confinement in the Novatron mirror machine
- J. Scheffel, J. Jäderberg, K. Bendtz et al.
- The IFMIF-DONES Irradiation Modules F. Arbeiter, U. Wicek, B. Brañas et al.
- Numerical study of thermohydraulics induced by highly under-expanded jet during in-vessel LOCA for the CFETR WCCB concept

Jinghua Jiang, Jun He, Tianyu Chen et al.



Nucl. Fusion 65 (2025) 066010 (17pp)

# Multi-device analysis of energy loss duration and pellet penetration with implications for shattered pellet injection in ITER

G. Bodner<sup>1,\*</sup>, N. Eidietis<sup>1</sup>, Z. Chen<sup>2</sup>, P. Heinrich<sup>3</sup>, J. Herfindal<sup>4</sup>, S. Jachmich<sup>5</sup>, G. Papp<sup>3</sup>, J. Kim<sup>6</sup>, M. Lehnen<sup>5,†</sup>, U. Sheikh<sup>7</sup>, I. Coffey<sup>8</sup>, O. Ficker<sup>9</sup>, S. Gerasimov<sup>8</sup>, V. Kachkanov<sup>8</sup>, C. Reux<sup>10</sup>, S. Silburn<sup>8</sup>, H. Sun<sup>8</sup>, the ASDEX Upgrade Team<sup>a</sup>, JET Contributors<sup>b</sup> and the EUROfusion Tokamak Exploitation Team<sup>c</sup>

E-mail: bodnerg@fusion.gat.com

Received 3 February 2025, revised 7 April 2025 Accepted for publication 28 April 2025 Published 9 May 2025



#### Abstract

A robust disruption mitigation system (DMS) requires accurate characterization of key disruption timescales, one of the most notable being the thermal quench (TQ). Recent modeling of shattered pellet injection (SPI) into ITER plasmas, using JOREK and INDEX, suggests long TQ durations (6–10 ms) and slow cold front propagation due to the large plasma size. If validated, these predictions would have an impact on the desired pellet parameters and mitigation strategies for the ITER DMS. To resolve these questions, a database of SPI experiments from several small-to-large sized devices (J-TEXT, KSTAR, AUG, DIII-D, and

Author to whom any correspondence should be addressed.



Original content from this work may be used under the terms of the Creative Commons Attribution 4.0 licence. Any

further distribution of this work must maintain attribution to the author(s) and the title of the work, journal citation and DOI.

<sup>&</sup>lt;sup>1</sup> General Atomics, San Diego, CA, United States of America

<sup>&</sup>lt;sup>2</sup> Huwang University of Science and Technology, Wuhan, China

<sup>&</sup>lt;sup>3</sup> Max Planck Institute for Plasma Physics, Garching, Germany

<sup>&</sup>lt;sup>4</sup> Oak Ridge National Laboratory, Oak Ridge, TN, United States of America

<sup>&</sup>lt;sup>5</sup> ITER Organization, St. Paul-lez-Durance, France

<sup>&</sup>lt;sup>6</sup> National Fusion Research Institute, Daejeon, Korea, Republic Of

<sup>&</sup>lt;sup>7</sup> École Polytechnique Fédérale de Lausanne, Swiss Plasma Center, Lausanne, Switzerland

<sup>&</sup>lt;sup>8</sup> United Kingdom Atomic Energy Authority, Culham Campus, Abingdon, Oxon OX14 3DB, United Kingdom of Great Britain and Northern Ireland

<sup>&</sup>lt;sup>9</sup> Institute of Plasma Physics of the Czech Academy of Sciences, Prague, Czech Republic

 $<sup>^{\</sup>rm 10}$  CEA-IRFM, St. Paul-lez-Durance, France

<sup>†</sup> Deceased.

<sup>&</sup>lt;sup>a</sup> See Zohm *et al* 2024 (https://doi.org/10.1088/1741-4326/ad249d) for the ASDEX Upgrade Team.

b See Maggi et al 2024 (https://doi.org/10.1088/1741-4326/ad3e16) for JET Contributors.

<sup>&</sup>lt;sup>c</sup> See Joffrin *et al* 2024 (https://doi.org/10.1088/1741-4326/ad2be4) for the EUROfusion Tokamak Exploitation Team.

JET) has been compiled under the auspices of the International Tokamak Physics Activity MHD, disruptions, and control topical group. Analysis of the energy loss duration (proxy for the TQ duration) with machine size is presented for both mixed neon/deuterium (Ne/D) SPI and pure deuterium (D) SPI. Several metrics for the energy loss onset (e.g. soft x-ray signal drop,  $I_p$  dip, and radiation flash) were considered as the conventional metric, electron cyclotron emission, is often cut-off during SPI. Several scalings with different onset metrics showed an increase in energy loss duration with machine size. The energy loss duration was additionally shown to be a function of the ratio between the number of SPI neon atoms injected and the stored energy. Analysis of the pellet shard position relative to the cold front found that in larger devices, pellets are typically found inboard of the q=2 surface at the energy loss onset. Lastly, the delay between the pellet shards hitting the q=2 surface and the energy loss onset was additionally found to increase with machine size. This suggests that the pellet shards in large devices will penetrate faster and further than the cooling front.

Keywords: disruption mitigation, shattered pellet injection, thermal quench, disruption, ITER

(Some figures may appear in colour only in the online journal)

#### 1. Introduction

Plasma disruptions are one of the largest barriers to the tokamak as a cost-effective fusion reactor. Disruptions result in the rapid loss of plasma thermal and magnetic energy. If unmitigated, the impact of this energy to the first wall can severely damage the plasma-facing components leading to costly down time. Apart from JET with the ITER-like wall [1], current tokamaks can withstand unmitigated disruptions. ITER [2, 3], SPARC [4], and future pilot plants will all have larger stored energies and plasma currents that will necessitate robust disruption mitigation systems (DMSs).

In ITER, disruption mitigation will be done primarily using shattered pellet injection (SPI) [5]. Here, frozen pellets (typically a combination of hydrogen, deuterium, and/or neon) are shattered and injected into the plasma to quickly radiate the plasma energy uniformly over the first wall. The pellets are shattered prior to entering the plasma to increase the particle assimilation. In preparation for ITER operation, SPI systems have been successfully deployed on several tokamaks around the world [6–12].

While SPI has been routinely tested on a wide range of tokamaks, the ITER SPI system represents a large extrapolation in our understanding of disruption mitigation. The ITER DMS will feature much larger pellets (28 mm diameter) that will be injected into plasmas with much larger sizes  $(V_{\text{plasma}} = 830 \text{ m}^3)$ , plasma currents  $(I_p \leq 15 \text{ MA})$  and stored energies ( $W_{\text{MHD}} = 36 \text{ MJ}$  in L-Mode). For reference, the SPI system on JET injects 4.6-12.5 mm diameter pellets into plasmas with  $V_p = 78 \text{ m}^3$ ,  $I_p = 1-3 \text{ MA}$ , and  $W_{\text{MHD}} \leq 8 \text{ MJ}$ . While the ITER DMS design has been finalized, there are still many open questions about the expected performance of the system. To address these questions, the fusion community has developed several modeling codes to predict SPI performance in ITER, namely JOREK [13, 14], INDEX [15], NIMROD [16], M3D-C1 [17], and DREAM [18]. These codes vary in their speed, fidelity, and methodology, but their combined use allows for accurate evaluation of current SPI experiments and prediction of future SPI performance.

JOREK and INDEX, in particular, have been used to simulate mixed Ne and D SPI (referred to here as Ne/D) and pure D SPI discharges in AUG, DIII-D, KSTAR, and JET and have shown good consistency with experiment [19–23]. Recently, JOREK and INDEX have been used to simulate SPI-triggered disruptions in ITER L-mode plasmas. These simulations predicted longer than expected thermal quench (TQ) durations on the order of 6-10 ms [24, 25]. In [24], it is argued that size effects may play a significant role in the increased TQ duration as the pellet ablation time is theorized to scale with the major radius and the toroidal field ( $\tau_{\rm abl} \propto R^{5/3} B^{0.842}$ ). A longer pre-TQ duration would provide more time for: the pellet shards to interact with the plasma, the dispersal of the plasma thermal energy, and subsequent pellet injections. In addition, these simulations have also predicted that the pellet shards will penetrate faster than the cold front, identified here as the radial position where the electron temperature  $(T_e)$  profile is 10 eV. This may result in improved particle assimilation (due to higher  $T_{\rm e}$  at the deposition location) and reduced RE seeds (due to lower  $T_e$  at the TQ onset). Both results would be beneficial for thermal load mitigation and may relax some of the mitigation constraints, thus it is imperative to validate these predictions.

SPI has such stringent mitigation constraints as the fragment arrival time can significantly impact the particle assimilation. Generally, the fragments need to be deposited into the plasma before the global reconnection event (GRE). The GRE characterizes the final stochastization of the flux surfaces and definitively signifies that all of the confined plasma thermal energy has been lost. Fragments injected after this point will assimilate poorly due to the very low plasma temperature and will only contribute minimally to the thermal load mitigation. Due to the unexpected and unavoidable nature of some disruptions, the warning time to the ITER DMS may be <10 ms [26]. Therefore, any extension to the pre-GRE or TQ duration

will be largely beneficial to the mitigation efficiency. It must be noted, however, that without a disruption precursor and adequate warning time, it will likely not be possible to fully mitigate the TQ loads even with the longer TQ duration estimates from JOREK/INDEX.

An empirical scaling of TQ duration (derived from the plasma temperature, pressure, or soft x-ray (SXR) emission) with machine size has been observed for both natural disruptions and MGI-triggered disruptions [2, 26], however, a comprehensive study of TQ durations in SPI-induced disruptions has not yet been performed. This paper seeks to remedy this and investigate the pellet penetration compared to the cooling front through the establishment of the International Tokamak Physics Activity (ITPA) MHD, disruptions, and control (MDC) 24 SPI database. The paper is organized as follows: section 2 details the composition of the ITPA MDC 24 SPI database and discusses the complexities of defining the TQ during SPI. Due to the differences in disruption characteristics for Ne/D SPI and pure D SPI, their analysis has been separated into two different sections. Section 3 presents the size scalings for Ne/D SPI and section 4 presents the size scalings for pure D SPI. Section 5 details the pellet penetration analysis and compares that to the inward movement of the radiative cold front. Lastly, section 6 provides some discussion of the results and concluding remarks.

#### 2. The ITPA MDC 24 SPI database

To investigate the scaling of SPI-induced TQ duration with machine size, a multi-machine database was compiled from five tokamaks of different sizes: J-TEXT, KSTAR, AUG, DIII-D, and JET. The approximate poloidal cross-sections of the included devices are plotted in figure 1 to show the difference in size between the devices (constant triangularity and elongation used for the diverted tokamaks). For each machine, relevant plasma parameters and diagnostic traces were collected from a number of SPI experiments that featured a range of different pellet parameters. The parameters and diagnostic traces compiled for the database are given in table 1. The database is comprised of 16 shots from J-TEXT, 2 shots from KSTAR, 14 shots from AUG, 73 shots from DIII-D, and 68 shots from JET.

In theory, electron cyclotron emission (ECE) provides the best indication of the plasma thermal energy loss due to its high temporal resolution measurement of the electron temperature. However, disruptions triggered by SPI can quickly become cut-off to ECE as the density can increase rapidly, leading the plasma to become evanescent. Therefore, there is not a standard community definition for the TQ onset time during SPI and alternatives to ECE are highly desired. These include the dip in the  $I_p$  signal before the  $I_p$  spike, the drop in SXR emission, the increase in the n=1 or n=2 signals, and the increase in the absolute extreme ultraviolet (AXUV), vacuum ultraviolet (VUV), and/or visible light signals associated with the radiation flash. Since we were unable to use ECE for many of the discharges in this database, we will refer to the

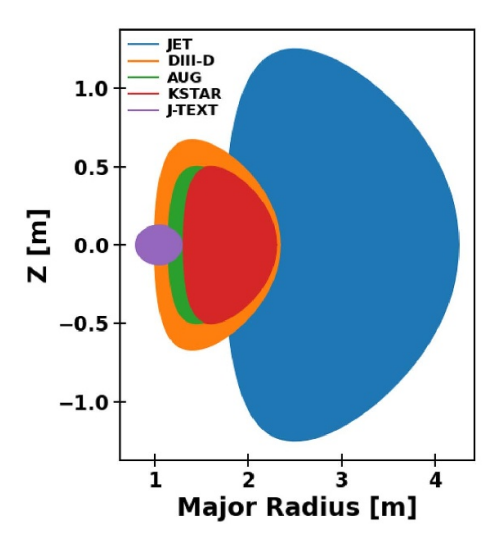
thermal loss timescale as the 'energy loss duration' rather than the 'TQ duration' to avoid possible confusion.

To assess the impact of various energy loss onset metrics on the size scaling, energy loss durations were calculated using all the metrics specified above. This resulted in a broad analysis of energy loss scalings and provided insights into potential alternative energy loss onset metrics for SPI experiments going forward. The energy loss duration was defined here as the time between the energy loss onset and the  $I_p$  spike. This definition was explicitly chosen due to ambiguity in the TQ duration without good ECE measurements. In the absence of these measurements, it can be difficult to determine not only the onset of the TQ, but the end of the TQ as well. We have therefore used the  $I_p$  spike as a proxy for the end of the TQ, as it represents the end of the GRE and the beginning of the current quench [27]. We acknowledge that this definition is likely an upper estimate for the energy loss duration, as it is possible that the thermal energy has been exhausted before the end of the GRE.

An example of how different onset metrics can produce different energy loss durations for the same shot is shown in figure 2. In this example, the  $I_p$  dip, the drop in the ECE signal at the q = 2 flux surface, the drop in the core SXR signal, and the increase in n = 2 amplitude were used to determine the energy loss onset time. The orange line corresponds to the pellet arrival time, the green line corresponds to the individually calculated energy loss onset times, and the black line corresponds to the  $I_p$  spike time. For the decreasing signals (ECE and SXR), the threshold for the energy loss onset was taken as a desired percentage of the baseline signal. For the increasing signals (n = 1 amplitude, n = 2 amplitude, and the radiation flash), an arbitrary percentage of the maximum signal was used as the threshold for the energy loss onset time. If the threshold occurred before the pellet arrival time or after the  $I_p$ spike time, the energy loss duration for that shot was not used. Figure 2 shows that the estimated energy loss duration can vary between 0.5 and 2.5 ms just based on the chosen onset metric and provides further motivation for the consideration of multiple onset metrics. Section 3 will detail the Ne/D SPI analysis and section 4 will detail the pure D analysis.

# 3. Size scaling of energy loss duration in Ne/D SPI

The analysis of Ne/D SPI and pure D SPI was separated due to the inherently different cooling mechanisms and disruption characteristics of the two pellet types [21]. Ne/D SPI shutdown is driven by strong radiation cooling which results in short pre-GRE durations (<5 ms). Pure D SPI, on the other hand, is dominated by dilution cooling (due to its low atomic number) which leads to a much less rapid loss of energy and very long pre-GRE durations (>10 ms). This can result in ambiguity in the TQ onset as pure D SPI discharges can have significant energy loss before the GRE [28]. This ambiguity is further complicated as several diagnostics become ineffective during pure D SPI. Comparing these two injection scenarios in the same analysis would therefore complicate energy loss duration estimates as different physical mechanisms and

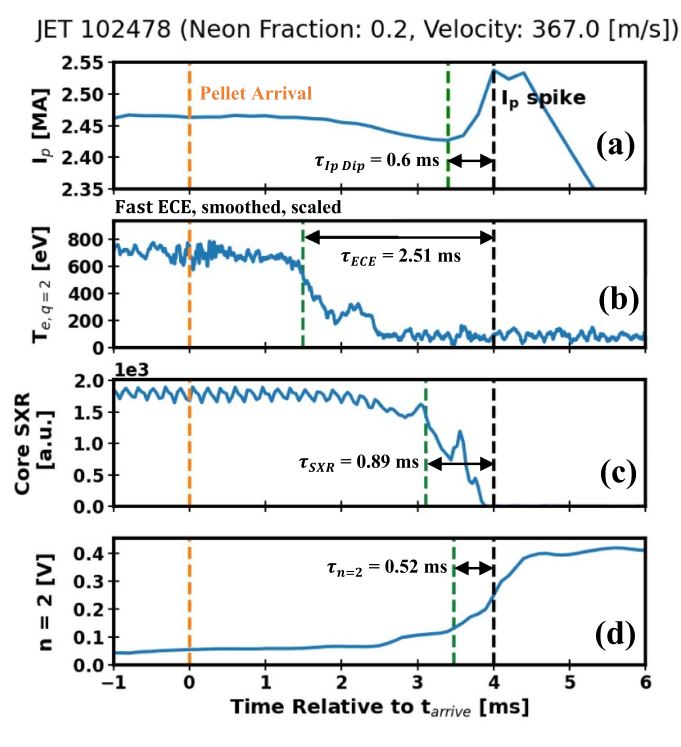


Machine	Minor Radius [m]	Major Radius [m]	Plasma Volume [m³]
J-TEXT	0.25	1.05	1.35
KSTAR	0.5	1.8	12
AUG	0.5	1.65	11.5
DIII-D	0.67	1.67	19
JET	1.25	3.1	78

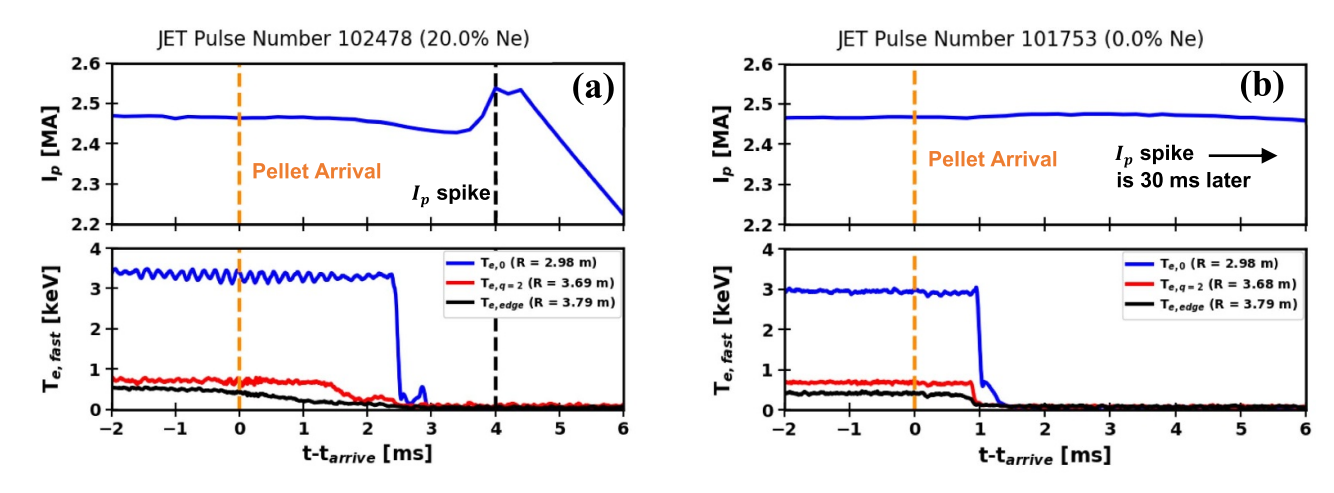
Figure 1. Size comparison and plasma parameters of tokamaks used in the ITPA MDC 24 database. Constant triangularity and elongation used for the diverted tokamak cross-sections.

Table 1. List of plasma parameters, SPI parameters, and diagnostics traces collected for the ITPA MDC 24 database.

SPI parameters	Plasma parameters	Diagnostic traces
Number of injected neon atoms	Toroidal field (T)	Plasma current (A)
Neon fraction	Major radius (m)	Stored energy (J)
Pellet velocity (m s <sup>-1</sup> )	Minor radius (m)	Line-average density (m <sup>-3</sup> )
Pellet arrival time (s)	Plasma volume (m <sup>3</sup> )	Radiated Power/AXUV/VUV (arb.
Pellet position, $\rho_{\text{pellet}}$ (t)	Normalized radius of the $q = 2$ surface	n = 1 magnitude (arb.)
	•	n = 2 magnitude (arb.)
		Soft x-ray (core, $q = 2$ , edge) (abr.)
		ECE (core, $q = 2$ , edge) (eV)



**Figure 2.** Examples of energy loss duration definition using four different metrics for the energy loss onset time: (a) the  $I_p$  dip, (b) 80% of the ECE signal at the q=2 surface, (c) 80% of the baseline core SXR signal, and (d) 20% of the maximum n=2 signal. Time base is relative to the pellet arrival time,  $t_{arrive}$ .



**Figure 3.** (a) Example of an electron temperature collapse in a JET Ne/D SPI discharge measured by ECE. (b) Example of ECE signal collapse in a JET pure D SPI discharge due to the plasma density surpassing the cut-off density threshold.

diagnostic limitations would be convolved. This section only presents data from discharges with Ne/D SPI.

#### 3.1. ECE

When available, ECE is the standard measurement to determine the TQ onset and TQ duration. ECE diagnostics can provide fast measurements (0.5–1 MHz sampling rates) of the electron temperature at several radial locations [29, 30], whereas other temperature diagnostics, such as Thomson scattering, are typically limited in their time resolution (1–5 kHz for systems with burst mode capability, <200 Hz for standard operation). As mentioned previously, the main drawback to ECE is its sensitivity to the plasma density. The ECE cut-off frequency, which causes the emitted radiation to be reflected away from the receiver, is dependent on the plasma density and at high densities the plasma can become evanescent to ECE. This is often the case in SPI experiments as the injected neutrals are quickly ionized, resulting in a large increase in the plasma density.

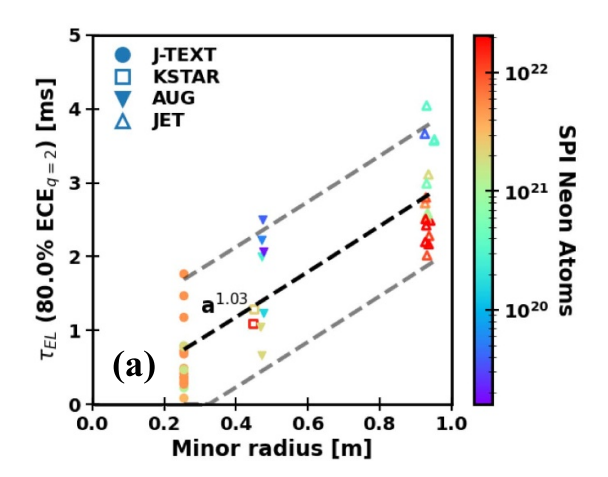
In an ideal scenario, the TQ should be visible in the ECE signal as an obvious decline in the electron temperature from the edge channels inward as the pellet shards penetrate through the plasma. This is shown in figure 3(a) for ECE measurements on JET featuring lines-of-sight at the plasma edge, the q=2 surface, and the core. When the plasma becomes cutoff to ECE, a rapid decline in temperature is observed regardless of radial location (assuming these locations are all above the cut-off density). An example of a JET plasma that has become cut-off to ECE and its resultant ECE measurements are shown in figure 3(b). Incorporating these cut-off shots into the database would lead to an overestimation of the TQ duration. Therefore, the database was filtered to only include shots that displayed evidence of a realistic temperature collapse (39 shots were filtered from the Ne/D SPI database).

As shown in figure 3, the ITPA database includes ECE signals from the edge, the q = 2 surface, and the core regions of

the plasma. While some energy loss is first observed in the plasma edge, it is widely believed that the TQ is not initiated until a large perturbation develops at the q=2 flux surface [2]. Additionally, if the high-density front is fast enough, the core ECE channels can become cut-off to ECE before the temperature drop is recorded. Therefore, the ECE channel viewing the q=2 surface was used as the metric for the energy loss onset time in this analysis. Specifically, the energy loss onset was estimated to be the time at which the ECE q=2 reached 80% of the baseline signal. This section will present energy loss durations from the ECE onset threshold to the  $I_p$  spike in order to keep consistency with the subsequent energy loss metrics. An analysis of the actual TQ duration scaling with the TQ onset and end defined by the ECE signal is presented in section 3.7.

The scaling of energy loss duration with minor radius (used here as a proxy for the machine size) for Ne/D pellets is shown in figure 4(a). Similar scalings were observed using the major radius and volume as the independent variable, however, minor radius showed better visual separation of the data and has been used in previous TQ duration scalings [2, 26]. Therefore, minor radius was chosen as the proxy for machine size here.

The Ne/D dataset was fit with a simple power law function,  $\tau_{\rm EL}=C*a^x$ . Here,  $\tau_{\rm EL}$  is the energy loss duration, C is a proportionality constant, a is the minor radius, and x is the scaling coefficient. The coefficients C and x are solved for given the empirical  $\tau_{\rm EL}$  and a values. The original error in the proportionality constant and the scaling coefficient ( $x=1.03\pm0.12$  and  $C=3.04\pm0.16$  for figure 4(a)) seemed low with respect to the observed spread in the data. Therefore, the error in the fit was taken as the standard deviations of each minor radius grouping (i.e. 0.3 m, 0.4–0.5 m, and 0.9 m) added in quadrature. This error was then added and subtracted to the fit and is represented by the dashed grey lines in figure 4(a). Negative energy loss durations in the dashed error bars were set to zero. With ECE as the energy loss onset metric, increased machine



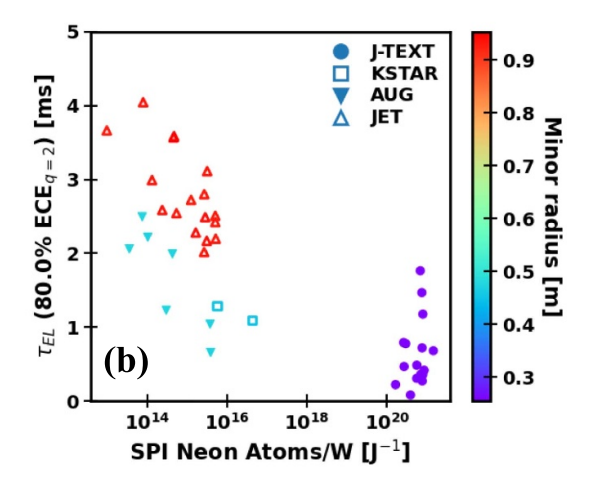


**Figure 4.** (a) Energy loss duration scaling with minor radius for Ne/D pellets. Energy loss onset time derived from 80% of the ECE q = 2 signal. Points colored by number of injected neon atoms. (b) Scaling of energy loss duration with the ratio of SPI neon atoms/ $W_{\rm MHD}$ . Points are colored by minor radius.

size led to increased energy loss duration with a considerable spread based on the number of injected neon atoms.

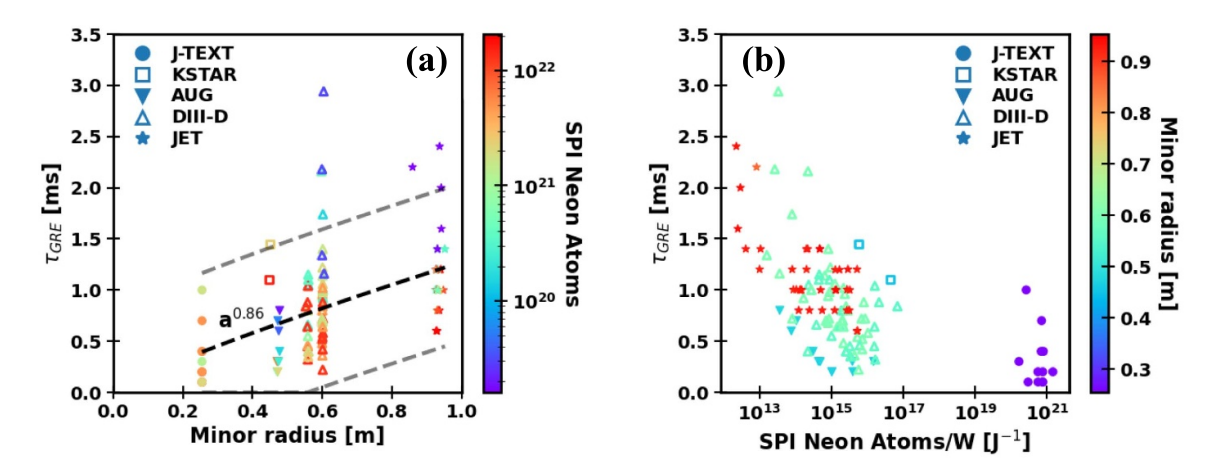
It is well known that the plasma stored energy and the SPI neon content have a large impact on the pre-GRE duration where the energy loss is dominated by radiation cooling. Higher energy plasmas will have longer pre-GRE durations and pellets with higher neon content will generally lead to shorter pre-GRE durations [8]. To assess the impacts of plasma stored energy and SPI neon content on the energy loss duration, figure 4(b) shows the energy loss scaling from figure 4(a) re-plotted with the ratio of neon atoms injected to the stored energy as the x-axis and with the points colored by the minor radius.

Figure 4(b) shows that increasing the ratio of SPI neon atoms/W<sub>MHD</sub> leads to shorter energy loss durations (as estimated by the ECE q = 2 signal). Similar trends were observed using the energy density as the normalizing parameter instead of the stored energy. Most notably, JET discharges with similar ratios of SPI neon atoms/W<sub>MHD</sub> to KSTAR and AUG discharges had significantly longer energy loss durations. This further supports the scaling trend from figure 4(a) and the JOREK/INDEX modeling results. There is a substantial gap in the data from  $10^{17}$  to  $10^{20}$  J<sup>-1</sup> due to the lack of ECE measurements from DIII-D (ECE is almost always in the cutoff regime during DIII-D SPI experiments). The following sections will introduce other energy loss onset metrics that can better address the duration scaling in this region. Nevertheless, this initial analysis supports the hypothesis from modeling that increased machine size leads to increased energy loss duration subject to the number of neon atoms injected and plasma stored energy. Assuming adequate warning time, large machines should seek to minimize the ratio of neon atoms injected to stored energy to achieve the longest energy loss durations. Of course, this ratio will need to be optimized against the radiation of the thermal loads. The next sections will explore if these scalings are consistent using other metrics for the energy loss onset time.

## 3.2. Ip dip (GRE)

Due to the uncertainty of ECE data quality during SPI, it is desirable to have alternative energy loss onset metrics. The  $I_{\rm p}$ dip time may serve as a useful alternative as all the included machines had some fast magnetics capability. The reduction in plasma current is due to a global stochastization of the flux surfaces which flattens the current profile and changes the plasma inductance. For this metric, the energy loss onset time was defined as the lowest  $I_p$  value between the pellet arrival time and the  $I_p$  spike. This definition is consistent with previous TQ studies such as those in [12]. While there can be significant energy loss before the GRE, this event is commonly understood to signify the final energy loss event due to the global stochastization of the flux surfaces. This metric is often used to determine the energy loss onset in pure D SPI where there is typically a very long gradual decay of thermal energy before the quench event.

The resulting GRE durations are plotted in figure 5 as a function of minor radius for Ne/D pellets. Figure 5(a) shows the general scaling of the GRE duration with machine size and figure 5(b) shows the impact of the SPI neon atoms/W ratio. The Ne/D GRE scaling exhibits a similar trend to the ECE q=2 scaling. Both scalings featured a general increase in the estimated energy loss duration with machine size. The main advantage to using the  $I_p$  dip as the onset metric was the inclusion of DIII-D discharges as well as discharges from other devices that may have been excluded due to cut-off ECE data. The DIII-D data appeared to be consistent with an approximately linear scaling of GRE duration and minor radius. The estimated GRE durations were slightly lower than the



**Figure 5.** (a) Scaling of GRE duration with minor radius for discharges with Ne/D pellets. Points are colored by number of injected neon atoms. (b) Scaling of GRE duration with the ratio of SPI neon atoms/W<sub>MHD</sub>. Points are colored by minor radius.

energy loss durations from the ECE scaling. This is expected as the GRE signifies the final energy loss event and does not account for thermal energy loss from dilution/radiation cooling that may occur before the GRE. Nevertheless, it is of note that the GRE duration shows a positive scaling with machine size which is consistent with the ECE energy loss duration scaling.

Regarding figure 5(b), the  $I_p$  dip scaling exhibited a slightly different behavior than the ECE q=2 scaling. Both scalings featured a decrease in energy loss duration with SPI neon atoms/ $W_{\rm MHD}$  ratio, however, the  $I_p$  dip scaling showed that DIII-D and KSTAR discharges can have similar energy loss durations to JET at similar SPI neon atoms/W ratios. Size effects may still be relevant, however, as it appears that the energy loss duration of JET discharges saturated at a minimum value around 0.7 ms regardless of the SPI neon atoms/W ratio.

## 3.3. SXR emission

While the  $I_p$  dip served as a useful energy loss onset metric to evaluate a larger number of discharges from the database, there are valid concerns to its relation to the thermal energy content. Therefore, it is of interest to have an additional energy loss onset metric that is related to the plasma thermal energy but features the same robustness as the  $I_p$  dip. This alternative metric has conventionally been the SXR signal which measures x-ray emission from the plasma in the general energy range of 0.1–3 keV [31]. SXR emission is directly related to the electron temperature of the plasma, however, this radiation is not as sensitive to the plasma density as ECE. The main concerns with SXR are that at low temperatures, the plasma may not emit x-rays with enough energy to penetrate the detector filter and radiation from the wall can make interpretation of the measurement difficult at times.

Similar to ECE, SXR signals were collected and analyzed at the edge, the q=2 surface, and the core regions of the plasma. In this analysis, however, the SXR channels viewing

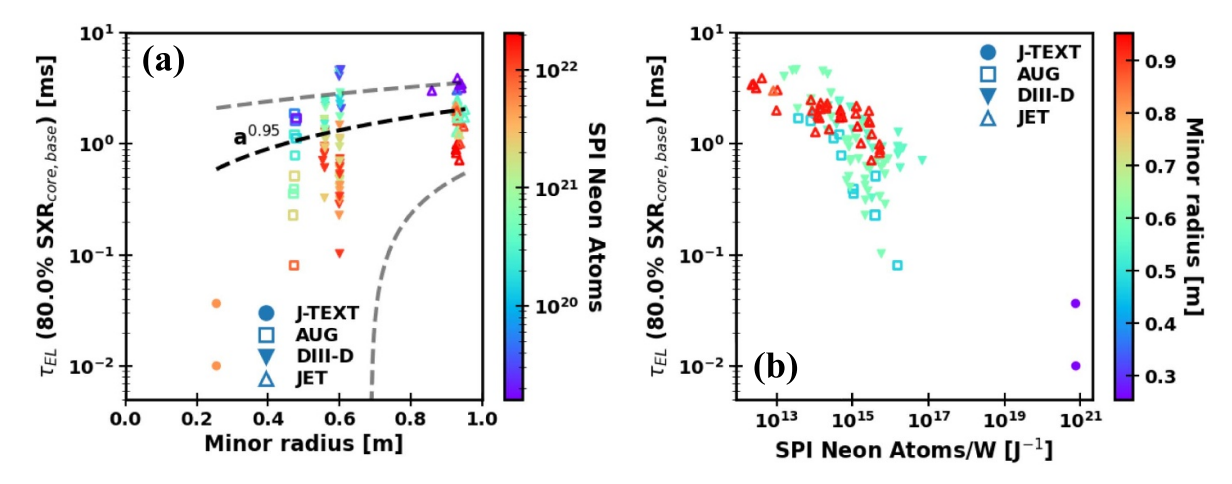
the plasma core were used to determine the energy loss onset instead of the q=2 channels. This was a consequence of diagnostic availability, as significantly more data was available at the core regions across machines than at the q=2 surface. The energy loss duration scaling using 80% of the baseline core SXR signal as the onset threshold is shown for Ne/D pellets in figure 6(a). A log scale is used here due to the very short energy loss durations for the J-TEXT discharges. Because of this log scale, the lower error bar appears to decrease exponentially to zero. Similar to the two previous metrics, the energy loss duration scaled almost linearly with the minor radius. A strong decrease in the energy loss duration with the SPI neon atoms/W ratio is shown in figure 6(b). Further evidence of a minimum energy loss duration for JET discharges was observed as well.

#### 3.4. n = 1 and n = 2 amplitudes

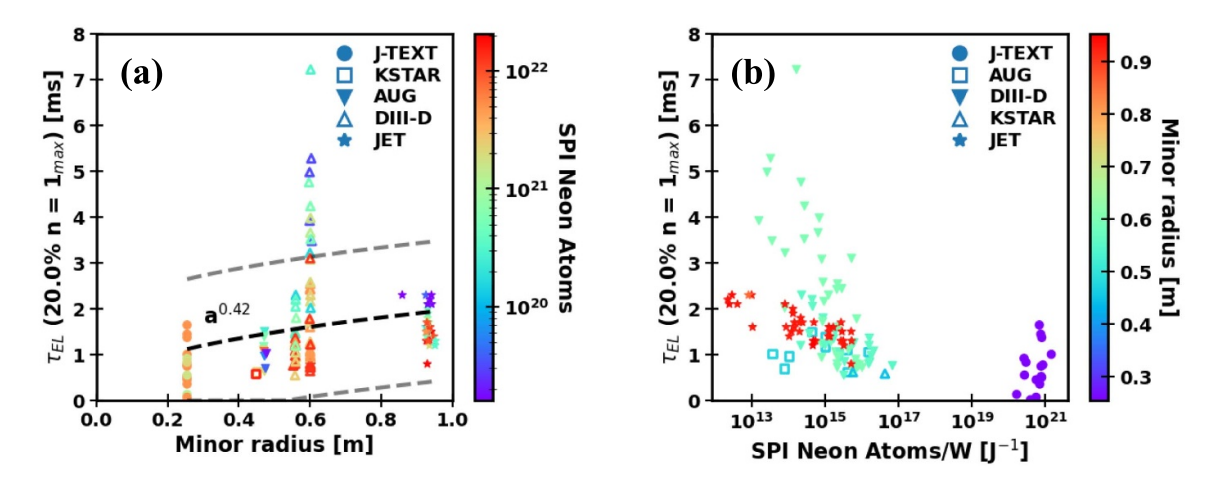
Disruptions have many different causes [32]; however, most lead to an excitation of an n = 1 or n = 2 mode which then grows rapidly and terminates the discharge. Therefore, we can use the growth of these instabilities as an indicator for the energy loss onset.

Figure 7(a) shows the energy loss duration scalings with the n=1 signal used as the onset metric for Ne/D pellets. 20% of the n=1 signal maximum was used for the energy loss onset time in both cases to provide a conservative estimate of the energy loss duration (lower threshold levels would result in longer energy loss durations). As mentioned previously, short energy loss durations make the mitigation of thermal heat loads more challenging and can result in increased damage if not fully mitigated. Therefore, the ITER DMS must be exceedingly cautious in its design and assume the most conversative estimates of energy loss duration where possible.

The relationship between energy loss duration and minor radius for this onset metric was difficult to interpret. The Ne/D pellets had a positive scaling coefficient of 0.44, however, this



**Figure 6.** (a) Energy loss duration scaling with minor radius for Ne/D pellets. Energy loss onset time derived from 80% of the core SXR signal. Points colored by number of injected neon atoms. (b) Scaling of energy loss duration with the ratio of SPI neon atoms/ $W_{MHD}$ . Points are colored by minor radius. Y-axis uses a log scale.



**Figure 7.** (a) Energy loss duration scaling with minor radius for Ne/D pellets. Energy loss onset time derived from 20% of the n = 1 signal maximum). Points colored by number of injected neon atoms. (b) Scaling of energy loss duration with the ratio of SPI neon atoms/ $W_{\rm MHD}$ . Points are colored by minor radius.

coefficient had a large error of  $\sim$ 50%. Therefore, it is difficult to definitively state that the energy loss duration for Ne/D SPI scales positively with the minor radius. Interestingly, when the energy loss durations were plotted against the SPI neon atoms/W ratio in figure 7(b), there were a large number of DIII-D discharges that had much longer energy loss durations than their JET counterparts. This may be a factor of the JET magnetic diagnostics, as none of the other onset metrics have given an indication that JET discharges have short energy loss durations (<2.5 ms) regardless of the neon content. Further investigation of these discharges shows minimal n = 1 and n=2 activity until very close to the  $I_p$  spike, which may be an indication of an additional delay between mode growth and mode detection. One possible hypothesis for this delay is the time resolution of the lowpass band filter. The JET fast magnetics system has a digitization rate of 10 kHz, however the lowpass band filter used in analog signal processing only has a time resolution of 6 Hz. Due to the large spread in n = 1energy loss durations, this onset metric is likely not a good candidate to project SPI energy loss dynamics to ITER.

A similar picture was observed when using the n=2 signal as the energy loss onset condition. The energy loss duration scaling for the Ne/D pellets is shown in figures 8(a) and (b) using the 20% signal maximum threshold. The n=2 dataset exhibited a weak positive scaling between energy loss duration and minor radius with large error, similar to the n=1 dataset. For the same reasons mentioned above, the n=2 signal is additionally not a good energy loss onset metric to project Ne/D SPI energy loss durations for ITER. Further analysis is needed to deduce why the JET energy loss durations from the n=1 and n=2 signal were so much lower than the estimates from the other onset metrics.

# 3.5. Radiation flash

Lastly, the radiation flash (i.e. the large burst of light commonly observed near the TQ) was considered as the final energy loss onset metric. Radiated power is a critical metric for SPI performance as it measures the efficiency and timescales

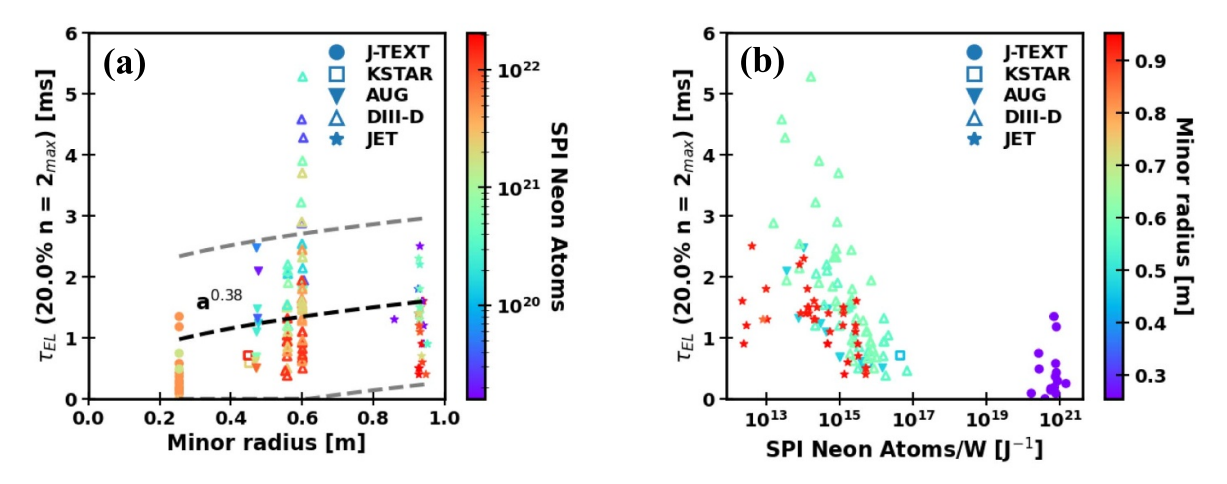


**Figure 8.** (a) Energy loss duration scaling with minor radius for Ne/D pellets. Energy loss onset time derived from 20% of the n = 2 signal maximum). Points colored by number of injected neon atoms. (b) Scaling of energy loss duration with the ratio of SPI neon atoms/ $W_{\rm MHD}$ . Points are colored by minor radius.

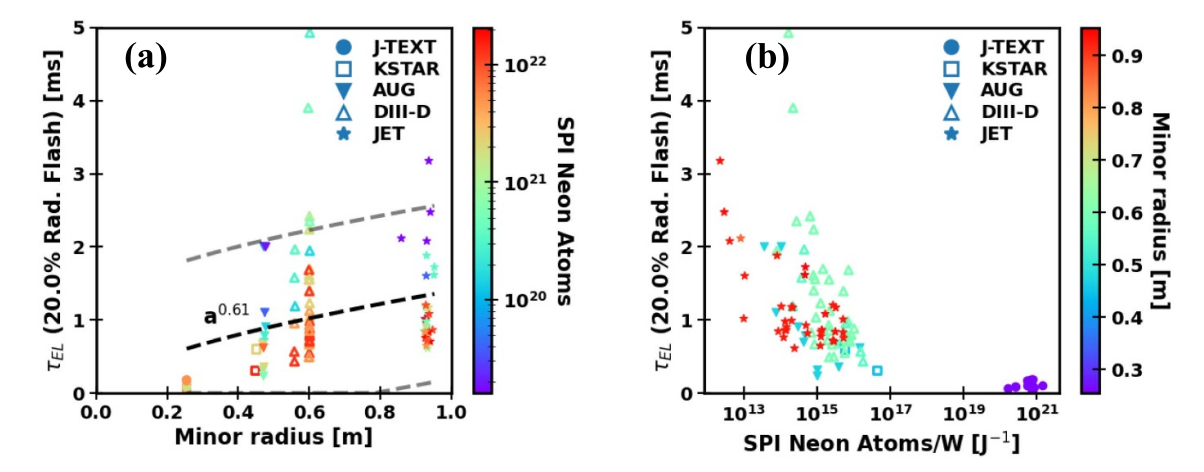


**Figure 9.** (a) Energy loss duration scaling with minor radius for Ne/D pellets. Energy loss onset time derived from 20% of the radiation flash maximum). Points colored by number of injected neon atoms. (b) Scaling of energy loss duration (using the radiation flash for energy loss onset) with the number of neon atoms injected divided by the plasma stored energy for Ne/D pellets. Points are colored by minor radius.

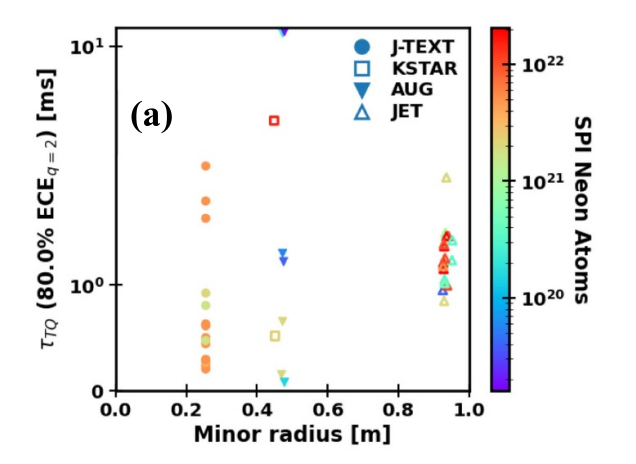
of the conversion of the plasma thermal energy into radiation. The radiation flash may be particularly useful as an energy loss onset metric for Ne/D SPI where radiative cooling is the dominant energy loss mechanism. In disruption experiments, the radiated power is derived from measurements of XUV emission using fast time response photodiode detectors as conventional foil bolometers are too slow to resolve the fast disruption dynamics. JET exclusively uses foil bolometers for radiated power measurements; therefore, the fast VUV photodiodes were used here to identify the radiation flash in JET SPI discharges.

The scaling of energy loss duration with minor radius using the radiation flash as the metric for the energy loss onset time is shown in figure 9(a). To maintain consistency with previous scalings, a 20% threshold of the peak signal intensity was used here for the energy loss onset. Scalings performed with 5% and 10% thresholds observed similar trends. Once again size effects were clearly observed in the energy loss duration. The resulting scaling coefficient of  $0.61 \pm 0.21$ , however, was

considerably weaker than those observed when using ECE, the  $I_{\rm p}$  dip, or SXR as the energy loss onset metric. Figure 9(b) shows the energy loss duration as a function of the SPI neon atoms/ $W_{\rm MHD}$  ratio. This figure is similar to that of figure 4(b) as the minimum energy loss durations for JET SPI discharges were consistently larger than the smaller machines at the same SPI neon atom/ $W_{\rm MHD}$  ratio.

# 3.6. TQ duration scaling of limited ECE dataset

As stated previously, ECE is conventionally used to determine the TQ duration when available. When using ECE, the onset and end of the TQ can be clearly identified. In these cases, the TQ onset proxy and the  $I_{\rm p}$  spike proxy are not needed. With the limited dataset that had valid ECE data, a TQ size scaling was created with the TQ duration defined as the time between the q=2 ECE signal drop from 80% of the baseline to 5% of the baseline. The scaling of TQ duration with machine size using the ECE q=2 signal is shown in figure 10.



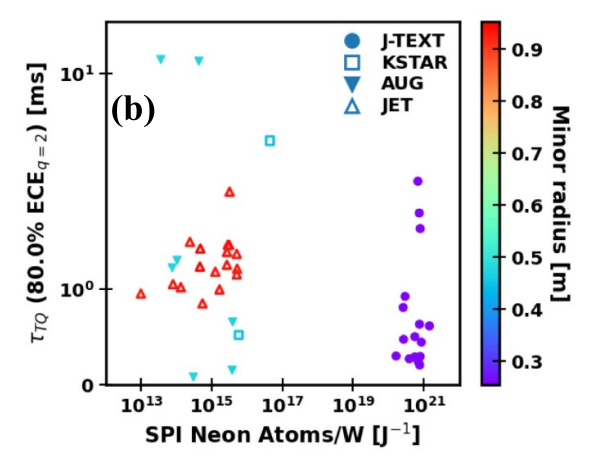


**Figure 10.** (a) TQ duration scaling with minor radius for Ne/D pellets. TQ duration defined as the time between 80% and 5% of the ECE q=2 signal. Points are colored by the number of injected neon atoms. (b) Scaling of TQ duration with the ratio of SPI neon atoms/ $W_{\rm MHD}$ . Points are colored by minor radius.

In this figure, there is not a clear size scaling for the small to medium sized tokamaks (J-TEXT, KSTAR, AUG). However, there is a clear increase in the minimum TQ duration for JET discharges relative to the small and medium tokamaks. This is consistent with the energy loss duration scalings presented earlier. Another notable feature is that there does not seem to be a clear dependence on the TQ duration with the amount of neon atoms injected. One hypothesis is that the energy loss during the TQ is largely driven by MHD and is therefore not dependent upon radiation cooling [12, 18]. It would appear then that a combination of size and radiation effects play an important role during the energy loss duration, but these effects may not have a large impact on the actual TQ duration. The most notable impact of the size effects on the actual TQ duration is the increase in minimum TQ duration for JET discharges. The limited size of the ECE dataset, however, makes it difficult to project these results to ITER.

#### 3.7. Energy loss scaling comparison and projection to ITER

The several energy loss scalings can now be compared and used to estimate a range of energy loss durations for ITER. This comparison is shown in figure 11 for Ne/D pellets. The markers are colored by the number of SPI neon atoms injected and each marker corresponds to the energy loss onset metric used for the scaling. The upper grey dashed line represents the error for the energy loss scaling with the longest ITER estimate (ECE  $\sim 7$  ms) and the lower grey dashed line represents the error for the scaling with the shortest ITER estimate (radiation flash  $\sim 0.9$  ms). The n=1 and n=2 scaling coefficients were excluded from this comparison due to the large error in their scaling coefficients.

The  $I_p$  dip, ECE, and SXR scalings had similar coefficients of 0.86–1, while the radiation flash scaling had a weaker coefficient of 0.61. The scalings predict energy loss durations in ITER to range from 0.9 to 7 ms depending upon the number of SPI neon atoms injected. Pellets with large amounts of neon (>10<sup>21</sup> atoms) would likely induce shorter

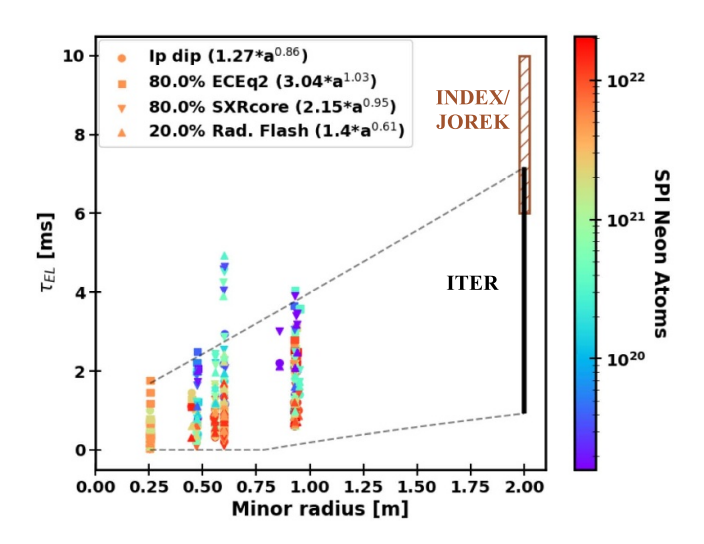


**Figure 11.** Comparison of energy loss duration size scalings for different onset metrics and their projections to the ITER minor radius. The marker type corresponds to the energy loss duration scaling, and the marker color corresponds to the number of neon atoms injected.

energy loss durations. In our opinion, these results are not consistent with the TQ durations from JOREK and INDEX simulations of 6–10 ms [24, 25]. The longest energy loss durations, which are likely an overestimation of the actual TQ durations, are on the lower end of the simulation range and those estimates correspond to a very low neon concentration. The modeling suggested that long TQ durations (>6 ms) would be achieved with  $5 \times 10^{22}$  neon atoms, which was more than any pellet in the ITPA MDC 24 database and would reside on the shorter end of the energy loss database prediction. Nevertheless, we do see evidence that size effects play a role in the energy loss duration and TQ dynamics.

To illustrate this role further, the energy loss duration has been plotted against the ratio of SPI neon atoms/ $W_{\rm MHD}$ , shown in figure 12. Here, the markers still correspond to their

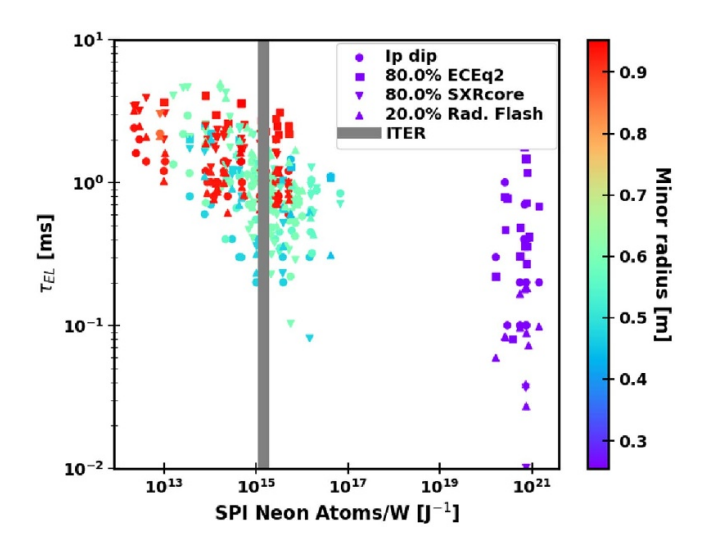


**Figure 12.** Comparison of energy loss duration size scalings with the SPI neon atoms/W ratio for different energy loss onset metrics and their projections to the ITER minor radius.

respective scalings but now they are colored by the minor radius (i.e. machine size). This figure is similar to those plotted in section 3, however, now all of the energy loss onset metrics are plotted together. We see that more SPI neon atoms led to shorter energy loss durations and larger machines (i.e. JET and ITER) may have a minimum energy loss duration. The grey bar represents the neon atoms to stored energy ratio for the modeling fiducials (5  $\times$  10<sup>22</sup> neon atoms/35 MJ) [24, 25]. For these parameters ( $\sim 10^{15} \, \mathrm{J}^{-1}$ ), JET discharges had a minimum energy loss duration of  $\sim 1$  ms. If there is some relationship between minimum energy loss/TQ duration and machine size, this would likely increase with the ITER minor radius and we may see minimum energy loss/TQ durations in ITER > 1 ms. This is somewhat consistent with the ablation time scaling from [24] which states that the pellet ablation time scales with  $R^{5/3}$  as larger pellets are required for larger devices. It is difficult at this time, however, to confirm predictions of  $\tau_{TO} > 6$  ms based on the limited ECE dataset that was available.

Lastly, it is important to note that the number of SPI neon atoms may not be the best quantity to consider when evaluating the impact of radiation cooling on the energy loss duration. Due to the rapidly evolving plasma dynamics during a disruption, only a fraction of the injected neon is ionized and assimilated into the plasma. This fraction is predominantly responsible for the radiation of the plasma thermal energy and thus may influence the energy loss duration more than the total injected number of neon atoms. Unfortunately, this metric was not available for majority of the discharges used in this database. Assimilated neon quantities (estimated using the 0D modeling code KPRAD [28]) were only available for ~60 JET discharges (different than the JET discharges included in the ITPA MDC 24 database).

Figure 13 shows a comparison of energy loss duration scalings for the JET assimilation database. Here, the energy loss duration is plotted against the ratio of assimilated neon atoms at the energy loss onset to the stored energy. The points are colored by the total number of neon atoms injected. It is

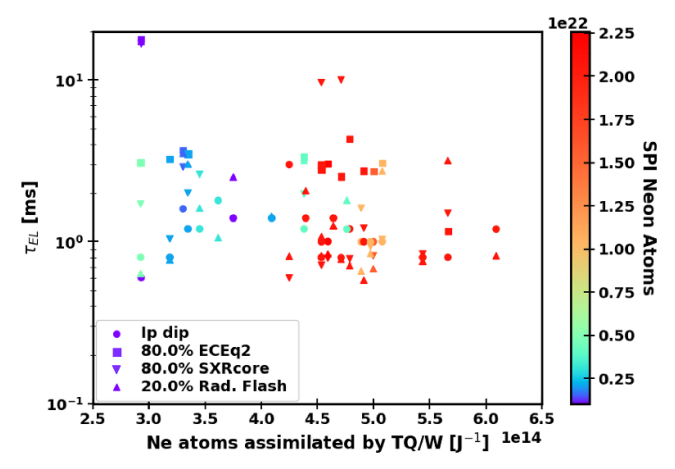


**Figure 13.** TQ duration vs. the neon assimilation fraction at the TQ (JET assimilation database only). Markers indicate the different energy loss onset metrics used.

difficult to make any definitive claims about the impact of assimilated neon atoms on the energy loss duration due to the large spread in the duration estimates (1–4 ms). No saturation in the amount of assimilated neon atoms was observed as larger numbers of injected neon atoms generally led to larger numbers of assimilated neon atoms. This increase in assimilated neon atoms, however, did not appear to significantly reduce the energy loss duration as expected. Furthermore, discharges with low amounts of assimilated neon atoms did not have systematically longer energy loss durations as one may additionally anticipate. One hypothesis for this observed lack of impact is that these JET discharges were already in a regime where the minimum energy loss duration was reached. Therefore, even lower amounts of assimilated neon atoms may be needed to observe significantly longer energy loss durations. Future analyses should extend this work to wider ranges of assimilated and injected neon atoms as well as other machines in the ITPA MDC 24 database to get a full picture of the impact of neon assimilation on energy loss duration.

# 4. Size scaling of pre-GRE and GRE duration in pure D SPI

As mentioned previously, pure D SPI and Ne/D SPI have significantly different cooling mechanisms and disruption timescales. Pure D SPI relies on dilution cooling to gradually reduce the plasma thermal energy through collisions. This typically results in a large increase in density and a long, gradual energy loss leading up to the GRE, shown for both an AUG discharge and a JET discharge in figure 14.

While pure D SPI alone will not be sufficient for thermal load mitigation in ITER, it can be a useful tool to increase the density and reduce the stored energy before a subsequent mixed Ne/D injection. This is colloquially referred to as the staggered injection scheme and is a candidate scenario for ITER SPI [27]. All of these injections, however, need to take place during the pre-GRE phase in order to ensure sufficient particle assimilation. Because the initial injections must be

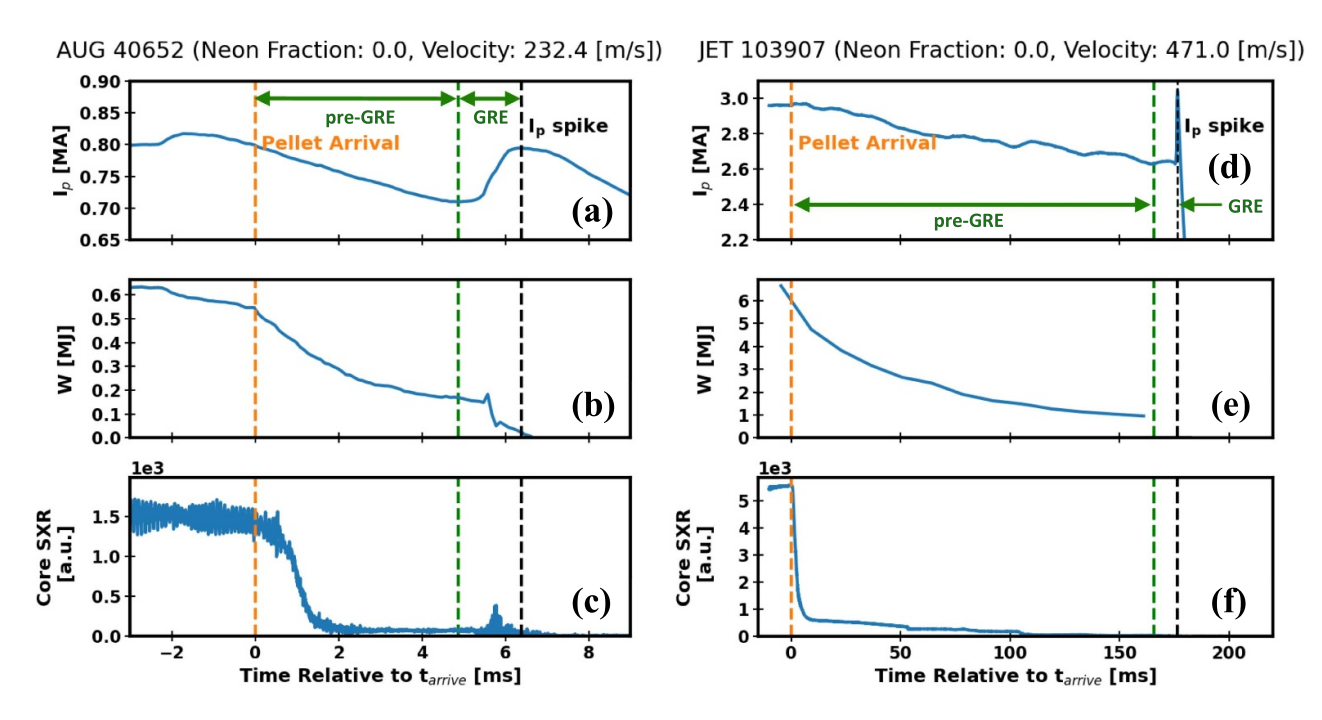


**Figure 14.**  $I_p$ ,  $W_{MHD}$ , and core SXR from an AUG discharge (a)–(c) and a JET discharge (d)–(f) with pure D SPI. The stored energy was observed to decrease significantly before the  $I_p$  dip time (green dashed line).

pure D, a scaling of pre-GRE duration with machine size is desired.

Due to the characteristics of pure D SPI, however, the energy loss onset metrics are limited. The gradual reduction in thermal energy and lack of quality ECE data (due to the increased  $n_e$ ) makes it difficult to designate the TQ or energy loss onset. As shown in figures 14(b) and (d), there can be a significant loss of energy before the GRE, however, the long timescale of this energy loss puts into question its characterization as a quench event. Additionally, the core SXR signal (a good alternative to ECE for Ne/D SPI) cannot be used here as the energy loss from pure D SPI results in lower energy xrays below the filter threshold. This is observed in the sharp decline of SXR signal in figures 14(c) and (f). Therefore, we will avoid the terminology of TQ in this section and consider only the pre-GRE and GRE durations as the relevant energy loss timescales. The pre-GRE duration is defined as the time between the arrival of the first pellet shards and the  $I_p$  dip. The GRE duration, as stated previously, is defined as the time between the  $I_p$  dip and the  $I_p$  spike. This section only presents data from discharges with pure D SPI.

#### 4.1. Pre-GRE duration

The scaling of pre-GRE duration ( $\tau_{\text{pre-GRE}}$ ) with minor radius is shown in figure 15(a). The pure D SPI dataset was limited in minor radius range as J-TEXT and KSTAR did not contribute any pure D SPI discharges to the database. There is a noticeable increase in the pre-GRE duration with minor radius, likely due to the larger stored energies of the JET discharges. This impact is clearly observed in figure 15(b) where the pre-GRE duration is plotted as a function of the stored energy. Here, the points are colored by energy density and projections to the

ITER stored energies of 35 MJ (ITER L-Mode) and 180 MJ (degraded ITER H-mode) are plotted as well.

The empirical scaling projects pre-GRE durations for ITER plasmas from 1 to 10 s depending upon the stored energy. These long durations, while encouraging, should be viewed as an upper bound and somewhat unrealistic as they are based on single pure D SPI into unseeded plasmas. Subsequent D injections and high levels of pre-SPI impurity seeding have been shown to reduce the pre-GRE duration for pure D SPI in JET [8, 28, 33].

Unrelated to the stored energy, there may be some additional evidence of size effects. In figure 15(b), several JET discharges had similar/longer pre-GRE durations than the DIII-D and AUG discharges even though the JET discharges had lower energy densities. Furthermore, two of these discharges (shown in purple) had lower stored energies and energy densities than several DIII-D discharges, but still had longer pre-GRE durations.

#### 4.2. GRE duration

The GRE duration of pure D SPI discharges is less relevant to ITER than the pre-GRE duration as pure D SPI alone is not envisioned for TQ mitigation. Nevertheless, the scaling of the pure D SPI GRE duration may still provide useful insights, especially for off-normal cases where pure D SPI is the only option for mitigation (e.g. failure of Ne/D pellets to launch).

The scaling of GRE duration with minor radius is shown in figure 16. A slightly positive trend in GRE duration is observed with machine size, however, it is difficult to make any strong conclusions to the limited minor radius range and proximity of the data. Interestingly, a large range of GRE durations (from 1 to 11 ms for JET discharges) were observed for discharges

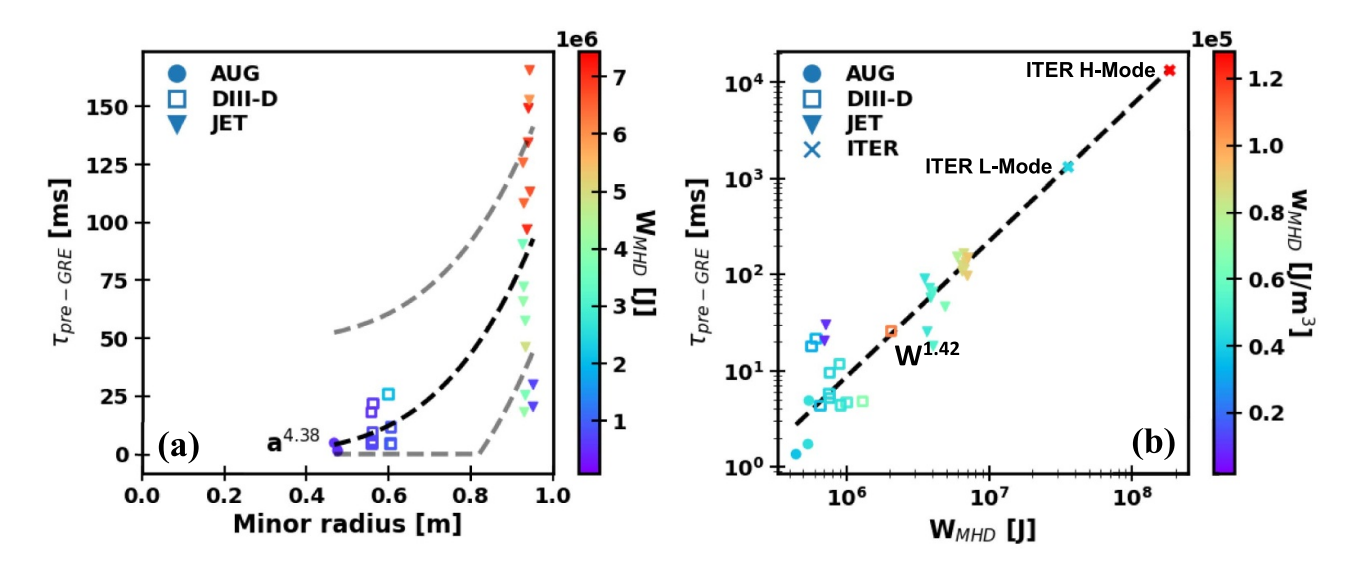


**Figure 15.** (a) Scaling of pre-GRE duration with minor radius. Points are colored by stored energy. (b) Scaling of pre-GRE duration with stored energy. Points are colored by energy density.

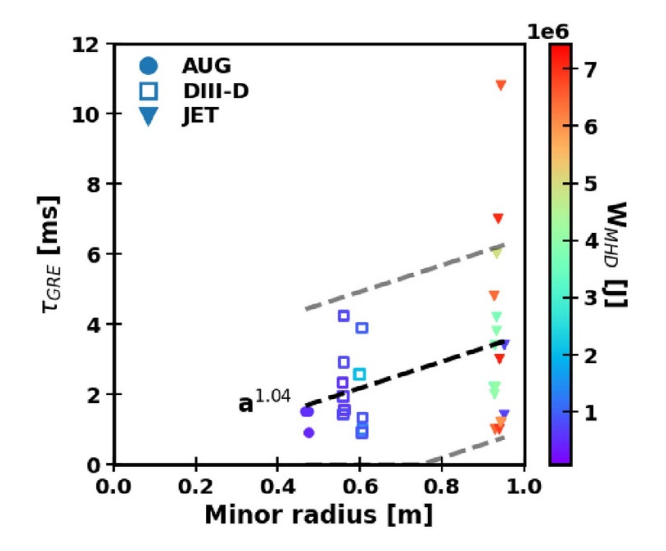


**Figure 16.** Scaling of GRE duration with minor radius. Points are colored by stored energy.

with similar stored energies. This may be related to differences in shard size, velocity, and penetration which may lead to different thermal energy levels at the onset of the GRE.

# 5. Pellet penetration with respect to the cold front

The second observation from the ITER SPI modeling was that the pellet shards would often penetrate faster than the radiative cold front [24, 25]. This would be beneficial from a mitigation standpoint as the pellet shards would ablate in a hotter region of the plasma potentially leading to increased assimilation and radiation fractions before the TQ was initiated. Increased assimilation would additionally result in lower core temperatures at the time of the TQ which would hopefully lead to less RE seeds.

In this analysis, the pellet position was determined from either fast camera images or estimated using the pellet speed and launch angle (these estimates were synced to the pellet arrival time at the q=2 surface from fast camera data). For the fast camera data, the pellet position is defined as the leading edge of the ablation cloud. This was done for all the shots in the ITPA MDC 24 database for which data was available. Calculating the position of the cooling front was a more challenging endeavor. As noted previously, the increase in density during the disruption event limits the capability of ECE. Therefore, analyses focused on using the relative pellet position to the q=2 surface at different times of interest during the TQ process to infer its position relative to the cooling front.

For example, with the limited ECE dataset, the q=2 cooling time was calculated to determine the time it takes for the cold front to reach the q=2 surface. The q=2 cooling time is defined here as the time between the first shards hitting the q=2 surface and the temperature at the q=2 surface dropping to 10 eV (illustrated in figure 17(a)). This is the same definition used in [25] which identified that faster pellets and larger shards give longer cooling times.

The calculation of the q=2 cooling time and its scaling as a function of minor radius are plotted in figures 17(b) and (c). Keeping in mind the limited dataset, the q=2 cooling time generally increased with the minor radius. In contrast to the INDEX modeling, there was not a clear relationship between pellet velocity and q=2 cooling time. This may be due to the difference in the number of neon atoms injected. In the JET discharges, which had relatively similar pellet velocities, pellets with higher numbers of injected neon atoms typically had shorter q=2 cooling times. One AUG discharge had a negative q=2 cooling time, implying that the ECE signal dropped to 10 eV before the pellet reached the q=2 surface. For AUG discharges, the pellet trajectory was synchronized with the pellet arrival time and determined purely from the measured pre-shattered velocity, the pellet trigger time,

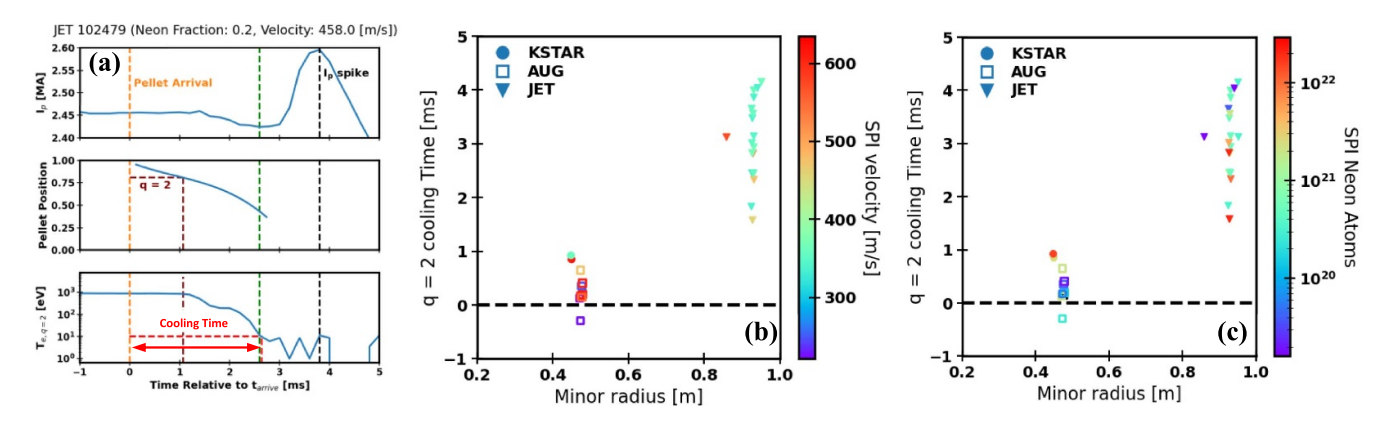


**Figure 17.** (a) Illustration of q = 2 cooling time definition. The brown line represents the pellet arrival at the q = 2 surface and the red line represents the time at which the ECE q = 2 channel drops to 10 eV. (b) Scaling of q = 2 cooling time with minor radius. Points colored by pellet velocity. (c) Scaling of q = 2 cooling time with minor radius. Points colored by number of injected neon atoms.

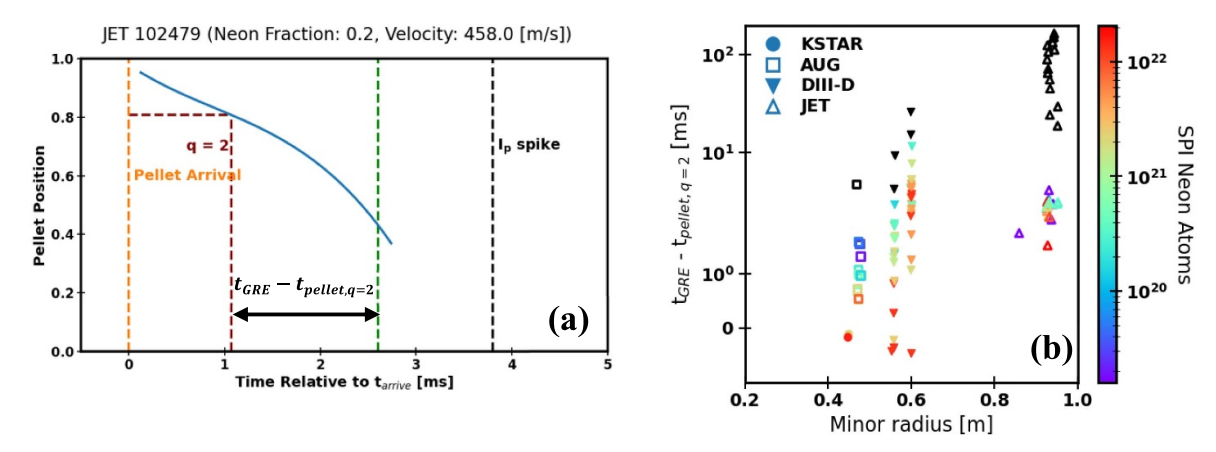


**Figure 18.** (a) Pellet trajectory illustrating the delay between the pellet shards hitting the q = 2 surface and the GRE onset. (b) Scaling of this timing delay with minor radius. Points colored by number of injected neon atoms. Points in black correspond to pure D pellets. Y-axis uses a symmetric log scale.

and the pellet arrival time (measured from AXUV). In some cases, the pellet trajectory needed to be shifted by multiple milliseconds to match the fragment arrival. These trajectories should therefore be viewed as crude 1st order approximations, rather than robust measurement quantities.

To include more discharges from the ITPA MDC 24 database, a metric for the pellet position relative to the cold front was developed that was not dependent upon ECE. Instead of using the time that the q=2 ECE signal drops to 10 eV as a proxy for the cold front position, one of the energy loss onset times from Section 3.2 was used. This was observed to be a good approximation in figure 17(a). The thought here is that at the energy loss onset, the radiative cold front would be somewhere outside of the core (when the cold front reaches the core, this signifies the end of the TQ). Therefore, the longer the delay between the pellets arriving at the q=2 surface and the TQ onset, the more time the pellets have to penetrate into the plasma before the TQ onset.

An example of the delay between the pellet crossing the q=2 surface and the energy loss onset determined by the  $I_p$  dip is shown in figure 18(a). These delays were computed for

all of the shots in the database with pellet tracking data and the results are shown in figure 18(b). Similar to figure 17(b), the timing delay between the pellet arriving at the q=2 and the onset of the energy loss increases with machine size. This suggests that large machines will likely have slowly propagating cold fronts which should give the pellet shards longer times in more ablation-conducive regions of the plasma. There was some evidence of the cold front penetrating faster than the pellet shards, however, this was confined to smaller devices with high neon SPI content.

The depth of the pellet penetration relative to the q=2 surface at the energy loss onset is shown in figure 19 for the same shots plotted in figure 18(b). The dataset in figure 18 is smaller than that of figure 18(b) as not all the pellets survived until the energy loss onset (this is especially true for the pure H/D pellets). In this figure, it is clear that all pellets in JET were likely inboard of the q=2 surface by the energy loss onset regardless of the pellet speed and Ne/D mixture. The picture is somewhat more complicated for smaller devices, which had pellets inboard and outboard of the q=2 surface for a variety of pellet velocities and Ne/D mixtures. Nevertheless, these

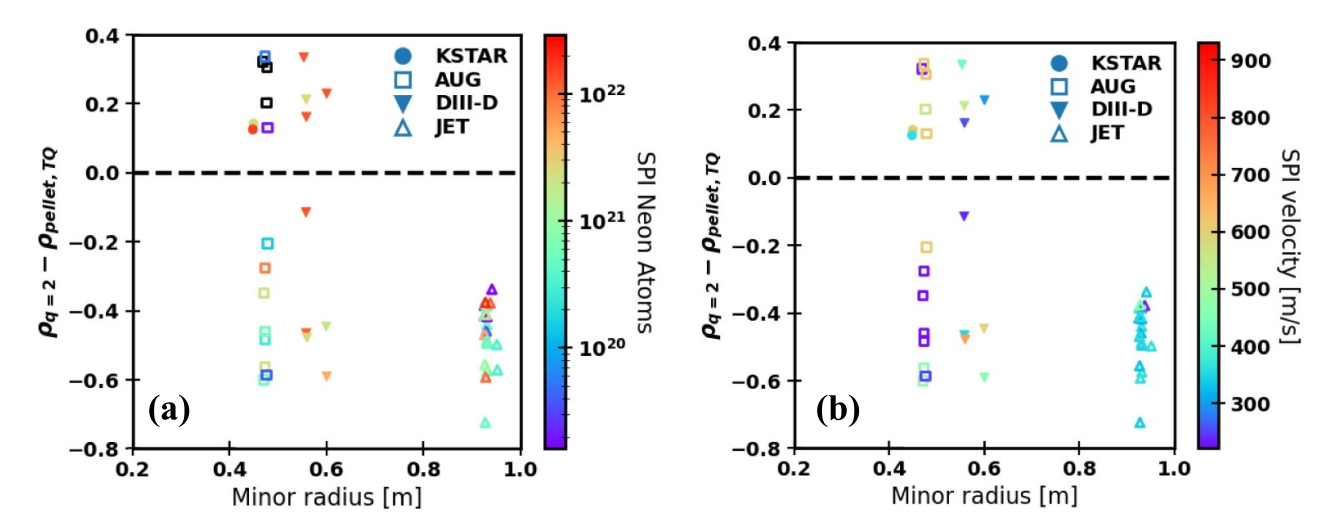


**Figure 19.** Pellet position at the onset of the GRE with respect to the q = 2 surface. (a) Points colored by number of neon atoms (b) points colored by pellet velocity. Negative values signify that the pellets are inboard of the q = 2 surface at the GRE onset. Points in black correspond to pure D pellets.

results support the modeling results that the pellet shards will likely penetrate faster and further than the cooling front in larger machines (e.g. JET, ITER, and DEMO).

#### 6. Conclusion

Understanding TQ dynamics will be crucial to disruption mitigation in ITER and future fusion pilot plants. To validate recent modeling of ITER SPI which suggested longer TQ durations and slow propagating cooling fronts due to size effects, a database of different sized tokamaks with SPI capability was assembled. This database contains discharges with various pellet velocities, Ne/D mixtures, and plasma thermal energies. Additionally, the database contains many diagnostic traces useful for determining the energy loss onset which allows for a wide characterization of possible machine size effects.

Analysis of this database has shown that the durations of SPI induced energy loss scaled positively with minor radius for several different energy loss onset metrics. It must be noted, however, that the resultant energy loss duration was largely impacted by the number of neon atoms injected. Higher amounts of injected neon atoms resulted in faster energy loss durations. Therefore, ITER will need to find the right Ne/D mixture that provides a lengthy pre-GRE duration but additionally radiates the required fraction of energy out of the plasma. For the range of SPI neon atoms in the database, the ITER energy loss duration was estimated to be in the range of 0.9-7 ms. This was not consistent with JOREK and INDEX modeling as the energy loss durations likely overestimate the TQ duration. Furthermore, the simulations predicted TQ durations of 6–10 ms with  $5 \times 10^{22}$  neon atoms which likely result in  $\tau_{\rm TQ} < 6$  ms according to the energy loss scalings from the database. Both the energy loss scalings and analysis of the limited ECE dataset, however, do show evidence of size effects and may set a minimum TQ duration for a given machine size, which would likely be  $\geq 1$  ms for ITER SPI.

Insights into potential energy loss onset metrics have additionally been found. ECE should remain the standard for TQ/energy loss duration measurements, however, in its absence the core SXR signal may be used as a suitable replacement. The beginning of the GRE ( $I_p$  dip) should continue to be a useful energy loss onset metric for Ne/D SPI if ECE and SXR measurements are unavailable, however this metric may lead to an underprediction of the energy loss duration. Using the n = 1 and n = 2 signals as TQ onset metrics proved to be challenging for this dataset and remain questionable as reliable metrics going forward.

Analysis of the limited pure D SPI dataset showed a strong scaling of pre-GRE duration with stored energy. This scaling projects very long pre-GRE durations for ITER up to 10 s in a degraded H-mode, however, these will likely not be realized due to the impact of subsequent D injections and assimilation issues due to pellet drifts. The GRE duration additionally scaled positively with machine size with no clear impact from the stored energy.

Lastly, the penetration of the pellet shards in relation to the radiative cold front was investigated. Modeling of ITER SPI predicts that the pellet shards will lead this cold front leading to enhanced assimilation/radiation and possibly inwardly convective heat transport. Analysis of the ITPA MDC 24 database showed that the q=2 cooling time increased with minor radius, suggesting that the cooling front propagates inwardly more slowly in larger devices. In addition to the cooling time, the delay between the shards arrival at the q=2 surface and the energy loss onset increased with machine size as well. It was difficult to determine if pellet velocity and/or the neon content ratio led to further penetration, but pellets injected into larger machines that survived until the energy loss onset were almost always determined to be inboard of the q=2 surface.

While this database was sufficient to provide some initial insights into the empirical energy loss scalings for SPI, the addition of more data points could significantly improve the

robustness of the conclusions. In particular, the database could be improved with more discharges from the small and medium tokamaks (J-TEXT, AUG, and KSTAR), low Ne/D and pure D SPI discharges from J-TEXT, and Ne/D SPI discharges from DIII-D with good ECE data. The results presented here motivate future analyses to understand the differences between the energy loss durations estimated by the ITPA MDC 24 database and those predicted from modeling. The increased energy loss duration estimated here further encourages the use of SPI for ITER and large sized fusion reactors.

## Data availability statement

The data that support the findings of this study are available from the corresponding author upon reasonable request.

#### **Acknowledgments**

The JET SPI experiments have been carried out as collaboration between EUROfusion and the ITER Organization. The JET SPI has received funding through the ITER project. The views and opinions expressed herein do not necessarily reflect those of the ITER Organization.

This work has been carried out within the framework of the EUROfusion Consortium, partially funded by the European Union via the Euratom Research and Training Programme (Grant Agreement No. 101052200—EUROfusion). The Swiss contribution to this work has been funded by the Swiss State Secretariat for Education, Research and Innovation (SERI). Views and opinions expressed are however those of the author(s) only and do not necessarily reflect those of the European Union, the European Commission or SERI. Neither the European Union nor the European Commission nor SERI can be held responsible for them.

This material is based upon work supported by the U.S. Department of Energy, Office of Science, Office of Fusion Energy Sciences, using the DIII-D National Fusion Facility, a DOE Office of Science user facility, under Award(s) DE-FC02-04ER54698, DE-SC0020299, and DE-AC05-00OR22725. This report was prepared as an account of work sponsored by an agency of the United States Government. Neither the United States Government nor any agency thereof, nor any of their employees, makes any warranty, express or implied, or assumes any legal liability or responsibility for the accuracy, completeness, or usefulness of any information, apparatus, product, or process disclosed, or represents that its use would not infringe privately owned rights. Reference herein to any specific commercial product, process, or service by trade name, trademark, manufacturer, or otherwise does not necessarily constitute or imply its endorsement, recommendation, or favoring by the United States Government or any agency thereof. The views and opinions of authors expressed herein do not necessarily state or reflect those of the United States Government or any agency thereof.

#### Conflict of interest

The authors have no conflicts to disclose.

#### **ORCID iDs**

- G. Bodner https://orcid.org/0000-0003-2497-9172
- N. Eidietis https://orcid.org/0000-0003-0167-5053
- P. Heinrich https://orcid.org/0000-0003-1823-5257
- J. Herfindal https://orcid.org/0000-0003-2846-597X
- G. Papp https://orcid.org/0000-0003-0694-5446
- M. Lehnen https://orcid.org/0000-0001-6043-8803
- U. Sheikh https://orcid.org/0000-0001-6207-2489
- O. Ficker https://orcid.org/0000-0001-6418-9517
- S. Gerasimov https://orcid.org/0009-0002-3793-7211
- C. Reux https://orcid.org/0000-0002-5327-4326
- S. Silburn https://orcid.org/0000-0002-3111-5113
- H. Sun https://orcid.org/0000-0003-0880-0013

#### References

- [1] Matthews G.F. *et al* 2016 Melt damage to the JET ITER-like Wall and divertor *Phys. Scr.* **2016** 014070
- [2] ITER Physics Expert Group on Disruptions, Plasma Control, and MHD and ITER Physics Basis Editors 1999 Chapter 3: MHD stability, operational limits and disruptions *Nucl. Fusion* 39 2251
- [3] Hender T.C. et al 2007 Progress in the ITER physics basis chapter 3: MHD stability, operational limits and disruptions Nucl. Fusion 47 S128–202
- [4] Sweeney R. *et al* 2020 MHD stability and disruptions in the SPARC tokamak *J. Plasma Phys.* **86** 865860507
- [5] Jachmich S. (the ITER DMS Design Team) 2022 The ITER disruption mitigation system design progress and validation IAEA 2nd Technical Meeting on Plasma Disruptions and their Mitigation (Cadarache, France)
- [6] Commaux N., Baylor L.R., Jernigan T.C., Hollmann E.M., Parks P.B., Humphreys D.A., Wesley J.C. and Yu J.H. 2010 Demonstration of rapid shutdown using large shattered deuterium pellet injection in DIII-D *Nucl. Fusion* 50 112001
- [7] Herfindal J.L. et al 2019 Injection of multiple shattered pellets for disruption mitigation in DIII-D Nucl. Fusion 59 106034
- [8] Jachmich S. et al 2022 Shattered pellet injection experiments at JET in support of the ITER disruption mitigation system design Nucl. Fusion 62 026012
- [9] Park S. et al 2021 Experimental results of multiple shattered pellet injection systems in KSTAR Fus. Eng. Des. 164 112200
- [10] Dibon M. et al 2023 Design of the shattered pellet injection system for ASDEX Upgrade Rev. Sci. Instrum. 94 043504
- [11] Li Y. et al 2021 Comparison of disruption mitigation from shattered pellet injection with massive gas injection on J-TEXT Nucl. Fusion 61 126025
- [12] Gerasimov S. et al 2024 Interaction of SPI pellets with plasma on JET and associated disruptions Phys. Scr. 99 075615
- [13] Hoelzl M. et al 2021 The JOREK non-linear extended MHD code and applications to large-scale instabilities and their control in magnetically confined fusion plasmas Nucl. Fusion 61 065001
- [14] Hu D. et al 2018 JOREK simulations of shattered pellet injection with high Z impurities 45th EPS Conf. Proc. (Prague, Czech Republic) p 4.1043 (available at: http://ocs. ciemat.es/EPS2018PAP/pdf/P4.1043.pdf)

- [15] Matsuyama A. et al 2021 Requirements for runaway electron avoidance in ITER disruption mitigation scenario by shattered pellet injection 2020 IAEA Fusion Energy Conf. (Virtual) p TH/3–12 (available at: https://nucleus.iaea.org/ sites/fusionportal/Shared%20Documents/FEC%202020/ fec2020-preprints/preprint0817.pdf)
- [16] Izzo V.A. et al 2011 Runaway electron confinement modelling for rapid shutdown scenarios in DIII-D, Alcator C-Mod, and ITER Nucl. Fusion 51 063032
- [17] Lyons B.C., Kim C.C., Liu Y.Q., Ferraro N.M., Jardin S.C., McClenaghan J., Parks P.B. and Lao L.L. 2019 Axisymmetric benchmarks of impurity dynamics in extended-magnetohydrodynamic simulations *Plasma Phys. Control. Fusion* 61 064001
- [18] Hoppe M., Embreus O. and Fülöp T. 2021 DREAM: a fluid-kinetic framework for tokamak disruption runaway electron simulations *Comput. Phys. Commun.* 268 108098
- [19] Tang W. et al 2024 Non-linear shattered pellet injection modelling in ASDEX Upgrade (arXiv:2412.03112)
- [20] Patel A. et al 2025 Modelling of shattered pellet injection experiments on the ASDEX Upgrade tokamak (arXiv:2312. 03462)
- [21] Lvovskiy A., Matsuyama A., O'Gorman T., Shiraki D., Herfindal J.L., Hollmann E.M., Marini C., Boivin R., Eidietis N.W. and Lehnen M. 2024 Density and temperature profiles after low-Z and high-Z shattered pellet injections on DIII-D Nucl. Fusion 64 016002
- [22] Lee S.-J., Hu D., Lehnen M., Nardon E., Kim J., Bonfiglio D., Artola F.J., Hoelzl M. and Na Y.-S. 2024 Nonlinear MHD modeling of neon doped shattered pellet injection with JOREK and its comparison to experiments in KSTAR *Nucl. Fusion* 64 106042
- [23] Bonfiglio D. et al 2022 Validation of 3D MHD simulation of mixed Ne-D<sub>2</sub> shattered pellet injection against H-mode experiments in JET 48th EPS Conf. Proc. (Maastricht,

- Netherlands) (available at: https://indico.fusenet.eu/event/28/contributions/245/attachments/259/967/epspaper\_bonfiglio.pdf)
- [24] Hu D., Nardon E., Artola F.J., Lehnen M., Bonfiglio D., Hoelzl M., Huijsmans G.T.A. and Lee S.-J. 2023 Collisional-radiative simulation of impurity assimilation, radiative collapse, and MDH dynamics after ITER shattered pellet injection *Nucl. Fusion* 63 066008
- [25] Matsuyama A., Hu D., Lehnen M., Nardon E. and Artola J. 2022 Transport simulations of pre-thermal quench shattered pellet injection in ITER: code verification and assessment of key trends *Plasma Phys. Control Fusion* 64 105018
- [26] Hollmann E.M. *et al* 2015 Status of research toward the ITER disruption mitigation system *Phys. Plasmas* **22** 021802
- [27] Lehnen M. 2024 ITER DMS—functional performance report Private Communication
- [28] Sheikh U. et al 2021 Disruption thermal load mitigation with shattered pellet injection on the Joint European Torus (JET) Nucl. Fusion 61 126043
- [29] Austin M.E. and Lohr J. 2003 Electron cyclotron emission radiometer upgrade on the DIII-D tokamak *Rev. Sci. Instrum.* 74 1457–9
- [30] de la Luna E., Sánchez J., Tribaldos V., contributors J.-E., Conway G., Suttrop W., Fessey J., Prentice R., Gowers C. and Chareau J.M. 2004 Electron cyclotron emission radiometer upgrade on the Joint European Torus (JET) tokamak Rev. Sci. Instrum. 75 3831–3
- [31] Alper B., Dillon S., Edwards A.W., Gill R.D., Robins R. and Wilson D.J. 1997 The JET soft x-ray diagnostic systems *Rev. Sci. Instrum.* 68 778–81
- [32] de Vries P.C., Johnson M.F., Alper B., Buratti P., Hender T.C., Koslowski H.R. and Riccardo V. 2011 Survey of disruption causes in JET *Nucl. Fusion* 51 053018
- [33] Sheikh U. et al 2025 Impact of impurity seeding on shattered pellet injections mitigations on the Joint European Torus Nucl. Fusion 65 036035